Journal of Materials Chemistry C

Accepted Manuscript

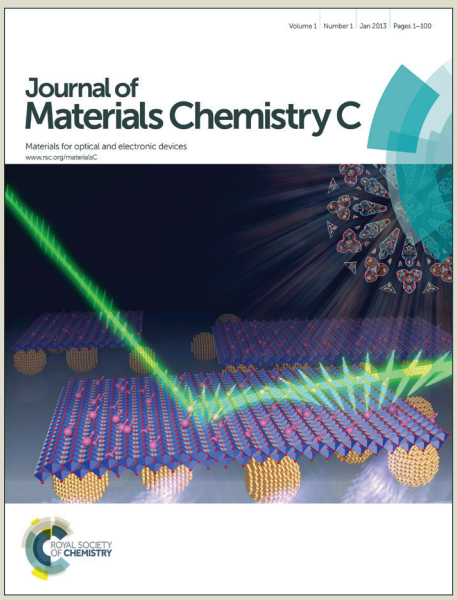

ROYAL SOCIETY OF CHEMISTRY

www.rsc.org/materialsC

Journal of Materials Chemistry C RSCPublishing

PAPER

Self-Organized Growth of Metallic Nanoparticles in a Thin Film under Homogeneous and Continuous-Wave Light Excitation

Cite this: DOI: 10.1039/xoxxoooooox

Received ooth May 2014,
Accepted ooth May 2014

DOI: 10.1039/xoxxoooooox

www.rsc.org/

Nathalie Destouches[a]*, Nicolas Crespo-Monteiro[a], Guy Vitrant[b], Yaya Lefkir[a], Stéphanie Reynaud[a], Thierry Epicier[c], Yang Liu[c], Francis Vocanson[a], Florent Pigeon[a]

Using a monochromatic plane wave to generate periodic arrays of metallic nanoparticles with tunable features buried in thin films is the original work we report here. We focus on the way such waveguiding metallic photonic crystals can self-emerge from thin films homogenously loaded with metallic precursors under a continuous-wave and homogeneous laser excitation. The paper fully describes the conditions leading to the formation of periodic structures and highlights the role of several parameters in the underlying physical mechanisms. The laser exposure parameters, especially, fix the geometrical and optical properties of the generated structures. Grating lines are parallel to the laser polarization and the period is directly linked to the laser wavelength. Both electron resonances of metal nanoparticles and optical resonances of guided modes interact to form the periodic patterns under homogeneous exposure. A model, based on the coupled mode theory, can be proposed to predict the spontaneous generation of such periodic nanostructures. It concludes that the guided waves exponentially enhance during illumination due to a positive feedback loop with the ordered growth of particles. This process opens new fabrication techniques for making optical devices and may found applications in various fields such as polarization imaging, displays, security or lighting.

1. Introduction

Long-range ordered nanoparticles lead to many electronic, optical, magnetic and chemical applications.[1] Many possibilities have been investigated to initiate self-ordering of materials. From an optical point of view, a great interest has emerged in the past decade to control and tailor optical properties, from the nanoscale to the macroscale, through the design and use of metallic nanostructures of various geometries[2,3] or the control of interactions between these individual nanostructures.[3] Arranged in periodic arrays, metallic nanostructures have an optical response strongly influenced by the near- and far-field coupling effects.[4] When the distance between nanostructures approaches their characteristic size, near-field coupling occurs and shifts of the particle plasmon resonance or extended plasmon modes can be observed.[5,6,7] Whereas, when the periodicity is on a length scale comparable to the wavelength of light, far-field coupling effects dominate the optical properties of the photonic crystal structure.[8] The situation where a metallic photonic crystal is combined with a waveguide is particularly interesting. Such a structure provides a strong interaction between the electronic resonance of the plasmon and the optical resonance of the quasi-guided mode of the structure, which can give rise to waveguide-particle-plasmon polaritons with a Rabi splitting.[9] The latter have been observed experimentally using 1D gold gratings elaborated by electron beam lithography on top of a guiding structure. The aim of our paper is to present a self-organization process that gives rise spontaneously to another kind of waveguiding metallic photonic crystals made of arrays of metallic nanoparticles buried in waveguides.

Creating the conditions so that matter naturally self-arranges under a uniform excitation is a guarantee of efficient and cost-effective processes. From a technological point of view, the latter generally come down to one-step processes.[10,11] But the physico-chemical mechanisms involved in self-organization of matter are always multiple and interactive, and their modeling and understanding remain usually delicate. For instance, uniform laser illuminations have been used to produce 1D laser-induced periodic surface structures, well known as LIPSS, on different kinds of homogenous materials.[11,12,13] The formation of LIPSS usually requires short laser pulses with high peak power. They form ripples on the material surface, whose orientation is linked to the laser polarization and whose period is a fraction of the laser wavelength. In the large number of articles on the subject it is commonly accepted that LIPSS originate from interferences between the incident beam and waves scattered or excited (surface plasmon polaritons) at the sample surface by heterogeneities.[14,15,16,17] Only few works deal

with metal-nanoparticle containing materials and they do not report any coupling with waveguide resonances.[18,19]
Here we show how a 1D metallic-nanoparticle grating embedded in a guiding layer can spontaneously emerge from a homogeneous optical waveguide, filled with ionic metallic precursors and few nanoparticle seeds, when it is illuminated by a homogeneous and continuous-wave (CW) laser beam. Conditions required on the material structure and properties and on the illumination parameters to generate such periodic nanoparticles' patterns are fully described. The influence of various parameters on the resultant structures is shown thanks to 2D and 3D characterizations at the nanoscale. Then, experimental spectra and electromagnetic simulations are used to prove the co-existence of both electron and optical resonances in the structures. The latter are used to propose a model that predicts the spontaneous generation of such structures. In this model, the self-arrangement of metal nanoparticles originates from interferences between the free-space incident radiation and guided waves. The model brings to the fore that guided waves exponentially enhance during illumination due to a positive feedback loop with the ordered growth of nanoparticles. We also highlight the fact that the nanoparticles' grating extends regularly when translating the waveguide under the laser beam, leading potentially to periodic arrays whose length is only limited by the substrate size.

2. Results and discussion

2.1. Film properties.

In the present study, the initial material is a mesoporous film of amorphous titania loaded with silver salt deposited on a glass substrate. The titania films were elaborated by a sol-gel process published previously and detailed in the experimental section.[20] They were 230±50 nm thick with pore sizes ranging from 5 to 20 nm. The films impregnated with an aqueous ammoniacal silver nitrate solution were transparent in the whole visible range and however photosensitive to high intensity visible light due to the spontaneous formation of few small (typ. <3 nm) silver nanoparticles after 12 hours in ambient conditions, as reported from TEM observations and low-frequency Raman spectra in reference [21]. Actually, despite their low absorption cross-section that prevents measuring significant absorption on such thin films, the small silver nanoparticles are at the origin of a temperature rise that can reach several hundreds of degrees. The latter occurs under high visible laser intensity and promotes the nanoparticle growth.[21] The film mesoporosity plays the role of a reservoir for the ionic silver precursor and ensures a high ionic mobility within the solid matrix; titania is used for its high refractive index since the films act actually as waveguides.

2.2. Formation of metallic nanoparticles' gratings.

The exposure of samples to a homogeneous and CW visible laser beam can lead to two opposite effects: (1) the photo-oxidation of silver nanoparticles as described in references [22,23,24], for instance, which leads to the decrease of the nanoparticle size, and (2) the sample heating through the excitation of the localized surface plasmon resonance (LSPR) of silver nanoparticles, which promotes the nanoparticles growth (it has to be noted that no heating occurs if nanoparticle seeds are absent from the TiO_2, even under 3 MW.cm^{-2} visible intensity).[21] The latter only occurs above an intensity threshold that was estimated to 10±1 kW.cm^{-2} at 488 nm in reference [21].

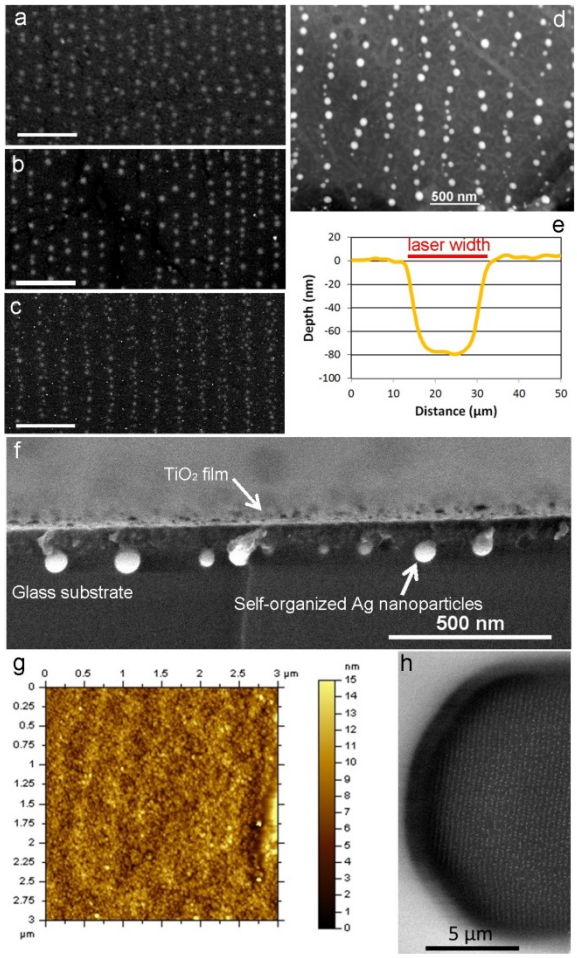

Fig. 1 (a-c) SEM pictures of samples illuminated with a translation speed of 0.3 mm.s-1 and at three different wavelengths: 488 nm, 514 nm and 647 nm, respectively. The scale bar is 1 µm. (d) High angle annular dark field scanning TEM micrograph of a sample illuminated at 488 nm and 3 mm.s^{-1}. (e) Film topography across a laser line drawn at 488 nm and 3 mm.s^{-1}. (f) SEM picture of sample "d" cross-section. (g) AFM picture of the sample "d" topography near the line center. (h) SEM picture of an end line showing the grating on the whole width.

We report here that the self-organization process we are dealing with only happens above this intensity threshold. In our experiments, the laser beam is slightly focused on the sample by a 10X microscope objective (Olympus MPlan N, N.A. 0.25), under normal incidence, to a circular spot with a typical $1/e^2$ diameter of 18 µm in the focal plane, which can be varied by changing the focus. This slight focusing is only performed to reach the intensity threshold needed to launch the process but is low enough to consider that the sample is illuminated by a quasi-plane wave. The incident power P_i on the sample is dependent on the laser wavelength λ_L as follows: 62 mW at 457 nm, 250 mW at 488 nm, 240 mW at 514 nm, 145 mW at 530 nm, 280 mW at 568 nm and 330 mW at 647 nm. During exposure, the samples are translated at a constant speed ranging from 0.05 to 30 mm.s^{-1} to draw few-millimeter-long lines with the laser beam. The self-organization process we report only takes place in a specific speed range going from 0.15 ± 0.1 mm.s^{-1} to 3 ± 2 mm.s^{-1} if we use wavelengths in the blue and green and 95 kW.cm^{-2} incident intensity. Slightly different limit values are obtained when using other wavelengths lying in the

LSPR band of silver nanoparticles, or other laser intensities. Under such illumination conditions, silver nanoparticles spontaneously grow and align along periodically spaced chains that form 1D nanoparticle gratings. Aligned bright dots corresponding to silver nanoparticles appear then on low magnification scanning electron microscopy (SEM - FEI Nova nanoSEM 200) pictures (Fig. 1a-c,h); these nanoparticles are buried in the titania film (Fig. 1f) and they become quite blurred at higher magnification. However, several features of the nanoparticle gratings can be inferred from SEM characterizations. The grating period increases with the laser wavelength and is always a fraction of it, as shown in Fig. 1a-c. A more precise estimate of the grating period is however deduced from optical measurements, as explained later. The orientation of the grating lines is parallel to the incident laser polarization and can be varied over 360° whatever the direction of the sample translation. Such sub-wavelength gratings extend over the entire surface of the illuminated area (Fig. 1h) and their period is homogeneous along the whole line drawn by moving the sample (few mm long). Transmission electron microscopy (TEM - Jeol 2010F) and high angle annular dark field scanning TEM provide more precise information on the nanoparticle size and shape. It resulted from statistical characterizations of different samples that silver nanoparticles have an average size ranging from 20 to 150 nm depending on the exposure conditions, and present a size distribution of several tens of nm on each sample. These electronic characterizations were completed by a tomography (see the Experimental section for details) performed with a dual-beam focused ion beam (FIB)/SEM system (Carl Zeiss Nvision40). This 3D view (see the Movie resulting from FIB/SEM measurements in supplementary information) shows that silver nanoparticles form in a plane located near the film substrate interface and rather spherical. Atomic force microscopy (AFM – Agilent Technologies 5500) showed that no significant periodic surface corrugation occurs on top of the embedded nanoparticle gratings (Fig. 1g). The surface roughness -root mean square height- of Fig. 1g is 2.2 nm. However, a large film compression can be measured in the whole illuminated area (Fig. 1e) by a surface profiler (Veeco Dektak 3ST). The film thickness can shrink by few nanometers to about 100 nm depending on the exposure conditions, especially because of the collapse of the mesoporosity during the laser-induced heating.

2.3. Spectral characterization.

Adjacent lines were drawn to cover a 9 mm² area for the measurements. The period Λ of each nanoparticle grating was calculated from measurements of the spectral position of the $\pm 1^{st}$ diffraction order emerging from the structure in a backscattering configuration, where the incidence angle was fixed to 45° and the diffracted one to -60°. These measurements give the average period (written in blue in Fig. 2) over the 9 mm² area with an accuracy of ±2 nm, and they confirm that the period increases with the laser wavelength.

We also report here the transmittance spectrum of few samples produced with a translation speed of 0.6 mm.s^{-1}, but various laser wavelengths (Fig. 2). Before exposure, the transmittance spectrum of the films under normal incidence is rather flat, independent on the probe beam polarization and close to 90% in the whole visible range.[21] After exposure, the spectra under normal incidence are polarization sensitive and exhibit the following features. With a probe beam polarized perpendicularly to the grating lines (⊥ polarization), a broad resonance (typ. 250 nm FWHM) leading to a decrease in the transmittance down to 20-40 % occurs in the spectrum around 450-500 nm. Its shape varies a little from one spectrum to the other, but its position is not really sensitive to the laser wavelength. With a polarization parallel to the grating lines (// polarization), a narrower resonance, whose spectral position is clearly correlated to the laser wavelength (Fig. 2a-e), is added to the broad resonance. A simple experiment can be implemented to better highlight the nature of both resonances; it consists in recording the transmittance spectrum under oblique incidence. All spectra have been recorded and exhibit a similar behavior, but only the more cogent (λ_L=647 nm), i.e. the one for which broad and narrow resonances are well separated, is shown. At an incidence angle of 5° or 10°, the broad resonance does not change significantly whereas the narrow one splits into two separated bands whose distance from the band recorded at 0° increases with the incidence angle (Fig. 2f).

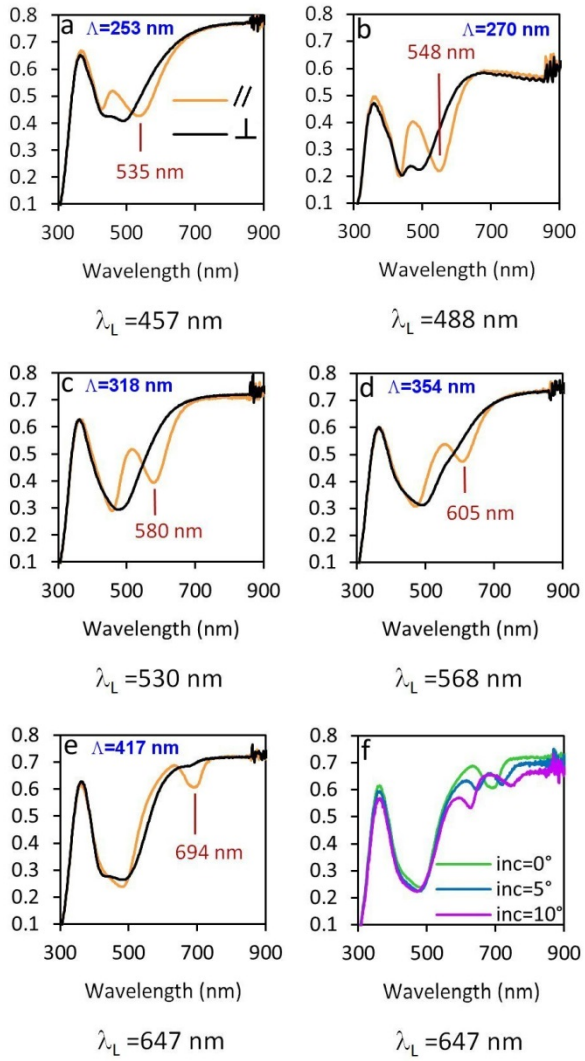

Fig. 2 Transmittance spectra under polarized light. (a-e) Spectra measured under normal incidence for // and ⊥ polarizations for samples produced with different laser wavelengths λ_L. The grating period Λ, deduced from optical measurements, is written in each graph as well as the position of the waveguide resonance that appears only for // polarization. (f) Spectra of sample "e" recorded under three different incidence angles for the // polarization.

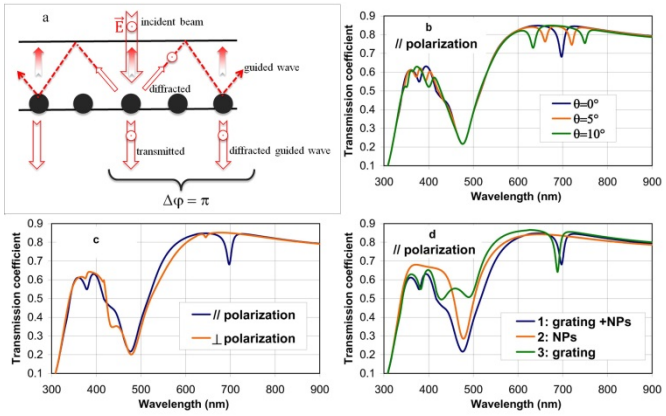

Fig. 3 (a) Sketch of the structure showing the principle of the waveguide resonance. When polarized parallel to the grating lines, the incident field is partly coupled to the forward and backward guided modes of the TiO_2 film through the ±1st diffraction orders of the nanoparticle grating. Then, these modes are diffracted back to free-space with a phase shift of π relative to the direct transmitted field causing destructive interferences in transmission. (b) Influence of the angle of incidence for // polarization on the simulated transmission spectra. (c) Spectra for // and ⊥ polarizations under normal incidence. (d) Contributions to the transmission spectrum of the grating (interference phenomena) and of the extinction of Ag NPs due to their plasmon resonance.

2.4. Electronic and optical resonances characteristic of waveguiding metallic photonic crystals.

Such results bring to the fore the presence of two different kinds of resonances in the system. The broad one is to result from the average of quadrupolar and dipolar plasmon modes of silver nanoparticles with a large size distribution; as an example the nanoparticle size ranges typically from 20 to 100 nm in the sample produced at λ_L=488 nm. This plasmon resonance is weakly sensitive to incidence angle and probably not to polarization either, according to the spectra of Fig. 2, and also because the nanoparticles are rather spherical, even if small near-field interactions between adjacent nanoparticles in each line cannot be ruled out totally.[25] On the other hand, the period and angular dependence of the narrower resonance is the signature of a waveguide resonance resulting from the excitation of a quasi-guided-mode (the guided mode of the TiO_2 layer becomes leaky -quasi-guided- in presence of the nanoparticle grating).[26] The latter usually gives rise in transmission to a sharp dip due to destructive interferences between the transmitted beam and the diffracted quasi-guided mode (Fig. 3a).[27] The high quality factor generally reported for such resonances is largely reduced here owing to scattering and absorption losses and also probably to the non-perfectly regular alignment of silver nanoparticles.[28] Electromagnetic modeling of the transmission coefficient of such nanostructures has been carried out with the differential method[29,30] taking into account diffraction of white light by the grating into the guided waves. The TiO_2 thin film is decomposed for modeling in two layers: (α) the upper one is TiO_2 with inclusions of Ag nanoparticles 4 nm in diameter to add losses. (β) the "grating" layer is formed by equivalent lines of bigger particles (35 nm in diameter) embedded in TiO_2. Calculations were performed by considering the parameters of the sample formed at λ_L=647 nm in Fig. 2e-f: Λ=417 nm and a film thickness of 155 nm (see Experimental for details). Although this modeling cannot accurately describe the shape of the plasmon resonance resulting from the presence of heterogeneous sizes of nanoparticles, the simulations (Fig. 3b-d) are in good agreement with the measured transmittance (Fig. 2e-f). Indeed, they highlight that under oblique incidence the excitation of the forward- and backward- propagating modes does not occur for the same wavelength and gives rise to two separated dips in the transmission coefficient, whose spectral distance increases with the incidence angle (Fig. 3b). This modeling also confirms the experimental observation that the grating cannot efficiently excite a guided mode under ⊥ polarization, leading only to a broad plasmon resonance (Fig. 3c) nearly as when the grating is absent (Fig. 3d). Simulations also show the excitation of higher order guided modes at lower wavelengths (around 400 nm) that cannot be observed experimentally due to the large LSPR band of the samples. It has to be noted here that the maxima of the modal field of such an asymmetric waveguide is located near the substrate interface. This may explain why the nanoparticles grow preferentially on this side of the film.

When spectrally overlapping as in Fig. 2a-d, the electronic and optical resonances can interfere and give rise to asymmetric line shapes that has already been observed in waveguiding metallic photonic crystals.[9] The precise characterization and modeling of such resonances, which can appear as Fano resonances,[31] is out the scope of the present article and will be dealt with elsewhere. We focus our attention here on the optical mechanisms that are likely to give rise to the formation of the nanoparticle gratings.

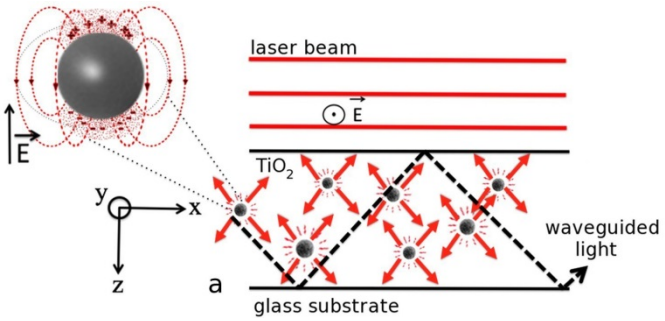

Fig. 4 Sketch of the system in the first moments of exposure: the TiO_2 film is loaded with silver salt and small silver nanoparticles that radiate as dipoles (close-up on the left, with a rotation of the electric field by 90° for a better visualization) predominantly in the plane perpendicular to the incident field $\vec{E}$. Most of the scattered waves escape the film (small arrows around each particle) but a part (longer arrows) remains confined inside the film in the form of a guided mode (dotted line).

2.4. Modeling the organized growth of nanoparticles under homogeneous light excitation.

The aim of the next section is to propose the outline of a model able to explain the optical origin of the mechanisms giving rise to the observed periodic structures. As said previously, the self-organization process only takes place above an intensity threshold that leads to a high temperature rise in the film, which promotes the nanoparticle growth. When growing, silver nanoparticles have an increasing scattering cross-section. The nanoparticles can then be considered as oscillating electric dipoles, which will interact in a reciprocal and constructive manner with the electric field confined in the TiO_2 waveguide, as explained below.

The incident laser beam is modeled by a plane wave polarized along $\vec{y}$ (Fig. 4). All electric fields and polarization vectors are thus oriented along $\vec{y}$, and this will not be indicated anymore.

The incident electric field writes $E_{inc} = E_0 e^{i(k_0 z - \omega t)}$. Taking into account reflections on various planar interfaces, the electric field present in the structure is called the "source field" and can be written in a general form $E_{src} = E_0 \psi_{src}(z) e^{-i\omega t}$. This field induces in the existing metallic nanoparticles $\vec{y}$-oriented oscillating electric dipoles, which mainly radiate in the x-z plane i.e. in the plane perpendicular to the incident polarization. This is an important feature since this explains why the interference pattern introduced below is always parallel to the incident laser polarization and thus why the lines of the nanoparticle grating are also parallel to this polarization. Furthermore, because the film is a waveguide, a part of the field scattered by metallic nanoparticles is trapped in the film. But only the particles periodically spaced by a distance $P = \frac{2\pi}{\beta_m}$, where β_m is the propagation constant of the guided mode, have to be considered as being phase-matched and able to excite the guided modes. As initially the nanoparticles are homogeneously distributed in the TiO_2 film, the amplitude of the guided modes is quite small, but not null.

Due to the involved orientations, only $\vec{x}$-propagating and $\vec{y}$-polarized guided waves can be excited. Let us call $A_m^{\pm}(x)$ the amplitude of the forward (+) and backward (-) $\vec{x}$-propagating TE guided waves. Their electric field writes $E_m^{\pm} = A_m^{\pm} e^{i(\pm\beta_m x - \omega t)} \psi_m(z)$ where $\psi_m(z)$ is the power-normalized wave function of the guided modes. These guided waves will interfere with the incident beam, giving rise to a total field in the film $E_{tot} = E_{src} + E_m^+ + E_m^-$ and creating a modulation along x of the light intensity inside the film. This spatial variation of the intensity has in return an influence on the nanoparticles evolution, which results in a feedback loop. As usually in such systems, if the feedback has the right characteristics, we can observe a growth of the grating. The aim of the formalism below is to study how the guided waves start to build and to point out the relevant conditions so that self-organization occurs.

Oscillating dipoles can be macroscopically described by a polarization density, whose expression is given by equation (1) when we consider that $\left|E_m^{\pm}\right| << \left|E_{src}\right|$:

$$P_{NP} \approx \varepsilon_0 \chi_{NP}(\vec{r}) E_{src} \qquad (1)$$

where $\chi_{NP}(\vec{r})$ is the variation of susceptibility of the film due to the growth of silver nanoparticles. We consider P_{NP} as a perturbation within the coupled-mode theory[32] and we obtain the usual equation:

$$e^{i(\beta_m x - \omega t)} \frac{dA_m^+}{dx} - e^{i(-\beta_m x - \omega t)} \frac{dA_m^-}{dx} = \frac{i\omega}{2} \int \psi_m(z) P_{NP}(\vec{r}) dz \qquad (2)$$

Anticipating that only the modulation amplitude at period $P = \frac{2\pi}{\beta_m}$ along x can coherently excite the guided modes, we can introduce the $\pm\beta_m$ Fourier components of the susceptibility perturbation as follows $\chi_{NP}(x,z) = \chi_{NP}^0(z) + \tilde{\chi}_{NP}^+(z) e^{+i\beta_m x} + \tilde{\chi}_{NP}^-(z) e^{-i\beta_m x}$ (y is an invariance axis). Because they find their origin in a modulation of the nanoparticle distribution, $\tilde{\chi}_{NP}^+$ and $\tilde{\chi}_{NP}^-$ have the same modulus and write $\tilde{\chi}_{NP}^{\pm} = \tilde{\chi}_{NP} e^{\pm i\varphi}$. With equations (2) and (1) we obtain:

$$\frac{dA_m^{\pm}}{dx} = \frac{i\omega\varepsilon_0}{2} E_0 \left\langle \tilde{\chi}_{NP}^{\pm} \right\rangle \qquad (3)$$

where $\left\langle \tilde{\chi}_{NP}^{\pm} \right\rangle = \int \psi_{src}(z) \psi_m(z) \tilde{\chi}_{NP}^{\pm}(z) dz$ and $\left\langle \tilde{\chi}_{NP} \right\rangle = \int \psi_{src}(z) \psi_m(z) \tilde{\chi}_{NP}(z) dz$ are overlap integrals of $\tilde{\chi}_{NP}$ with the source and guided mode fields. For the considered uniform excitation beam, the right-hand member of equation (3) is constant and integration is straightforward. More generally, we derive from this calculation that the guided wave amplitude is approximately given by equation (4) where w_{laser} is the $1/e^2$ diameter of the laser beam.

$$A_m^{\pm} = \frac{i\omega\varepsilon_0}{2} w_{laser} E_0 \left\langle \tilde{\chi}_{NP}^{\pm} \right\rangle \qquad (4)$$

This is for the electromagnetic part of the problem. The second part concerns the evolution of the nanoparticles under laser illumination. As discussed above, two mechanisms contribute to change the nanoparticle size and density: temperature-induced reduction leading to a nanoparticle growth and light-induced oxidation leading to a size decrease. These two contributions actually result in a change of the susceptibility perturbation controlled by the local intensity in the film. So, let us take into account the physical mechanisms influencing the nanoparticle evolution as described in equation (5):

$$\frac{d}{dt} \chi_{NP} = \eta I_{tot} \qquad (5)$$

χ_{NP} is therefore proportional to η and this will finally appear to be a crucial point. The total intensity in the film is modulated as:

$$I_{tot} = \left|\vec{E}_{tot}\right|^2 = \left|E_0 \psi_{src}(z) + A_m^+(x) \psi_m(z) e^{+i\beta_m x} + A_m^-(x) \psi_m(z) e^{-i\beta_m x}\right|^2 \qquad (6)$$

Using equation (6) in equation (5) we obtain after identification of the $e^{\pm i\beta_m x}$ terms:

$$\frac{d}{dt} \tilde{\chi}_{NP}^{\pm} = \eta E_0 \left[\psi_{src}(z) \psi_m^*(z) A_m^{\mp *}(x) + \psi_{src}^*(z) \psi_m(z) A_m^{\pm}(x)\right] \qquad (7)$$

With equation (4) and the definition of the overlap integral $\left\langle \tilde{\chi}_{NP} \right\rangle$ we obtain finally after some simple calculations:

$$\frac{d}{dt} \left\langle \tilde{\chi}_{NP} \right\rangle = -i\eta \frac{\omega\varepsilon_0}{2} \left|E_0\right|^2 w_{laser} \times \left[-\left(\int \left|\psi_{src}\right|^2 \left|\psi_m\right|^2 dz \right) \left\langle \tilde{\chi}_{NP} \right\rangle + \left(\int {\psi_{src}}^2 \left|\psi_m\right|^2 dz \right) \left\langle \tilde{\chi}_{NP} \right\rangle^* \right] \qquad (8)$$

Because the incident beam is propagating along z, ψ_{src} has a rapidly varying $e^{ik_0 z}$ phase term and the second term in the bracket of equation (8) can be neglected. This approximation is only done for sake of simplicity and does not have any influence on the final conclusions of this theoretical analysis. With this approximation, equation (8) becomes:

$$\frac{d}{dt}\left\langle \tilde{\chi}_{NP} \right\rangle = i\eta \frac{\omega\varepsilon_0}{2}\left|E_0\right|^2 w_{laser} I_{0\nu} \left\langle \tilde{\chi}_{NP} \right\rangle = i\eta C \left\langle \tilde{\chi}_{NP} \right\rangle \qquad (9)$$

where $I_{0\nu} = \int \left|\psi_{src}\right|^2 \left|\psi_m\right|^2 dz$ and the real constant coefficient C is given by $C = \frac{\omega\varepsilon_0}{2}\left|E_0\right|^2 w_{laser} I_{0\nu}$. This final equation explains why an organized nanoparticle grating structure with a period $P = \frac{2\pi}{\beta_m}$ can spontaneously emerge from an initially randomly distributed collection of small nanoparticles. Indeed, $\left\langle \tilde{\chi}_{NP} \right\rangle$ is the amplitude of the periodic modulation of the NP distribution and, according to equation (9) it will grow exponentially with time provided that:

$$\Im m(\eta) < 0 \qquad (10)$$

Therefore, this condition (10) appears to be crucial, and it depends on the relative predominance of the thermal and oxidation terms, which will be discussed in more detail in another paper. We finally find that the susceptibility perturbation grows at an exponential rate $\lambda = \frac{\omega\varepsilon_0}{2}\left|E_0\right|^2 w_{laser} I_{0\nu} \left|\Im m(\eta)\right|$. According to our analysis, we expect λ to be proportional to the laser irradiance, but also to the width w_{laser} of the laser beam. This is less obvious and comes from equation (4), showing that the process is expected to be more efficient if more space is allowed to the guided wave to coherently build.

This optical approach explains how the ordered growth of silver nanoparticles originates from interferences between the incident wave and guided waves excited by the growing nanoparticles themselves and how the growth of periodically spaced nanoparticles driven by the interference pattern enhances the contrast of the latter, in a positive feedback loop. More complex modeling will be developed in the future to link in a more quantitative manner the experimental parameters to the other physical mechanisms involved in such a self-organization process such as plasmon-induced thermal heating of the sample, heat-induced reduction of silver ions and nanoparticle growth, atomic diffusion, light-induced silver oxidation.

2.5. Extension of the grating during sample translation.

So far in the modeling, the sample was considered immobile relative to the laser beam. However, an interesting feature is the way the grating extends during translation of the sample. As interferences take place between the incident wave and guided waves excited by the structure in motion, the interference pattern moves at the same speed v as the sample itself, contrary to what would happen with classical lithography techniques where interferences are produced between to coherent beams independently of the sample. Indeed, taking the sample moving into account means replacing x by x-vt in equation (6), which leads, if we assume that the source field is much greater than the guided waves, to the following interference pattern:

$$\begin{aligned} I_{tot} &= \left|E_0\psi_{src}\right|^2 + \left|A_m^+ E_m\right|^2 + \left|A_m^- E_m\right|^2 \\ &+ 2E_0\psi_{src}\left|A_m^+ E_m\right|\cos\left[\beta_m(x-vt)+\varphi_m^+\right] \\ &+ 2E_0\psi_{src}\left|A_m^- E_m\right|\cos\left[\beta_m(x-vt)+\varphi_m^-\right] \end{aligned} \qquad (11)$$

where $A_m^{\pm} = \left|A_m^{\pm}\right| e^{i\varphi_m^{\pm}}$. The intensity modulation is therefore static relative to the sample, when the latter moves, and it simply extends on the edge of the already formed grating with a self-phase matching, leading to a regular period along cm or more. It has to be noted that once the first lines of a nanoparticle grating are formed, the guided mode is seeded by diffraction of the incident beam on the already existing lines. The contrast of the interference pattern is therefore higher during translation. The writing process does not need any stabilization procedure and can be used to write gratings whose length is only limited by the substrate size by just scanning the sample with the laser beam.

Moreover, once formed these nanoparticle gratings are quite stable upon subsequent exposures and even under high temperature rise. This is due to the crystallization of the TiO_2 film that occurs during the formation of nanostructures. These questions will be discussed in a next article.

3. Experimental

3.1. Film elaboration.

The samples consist of glass slides coated with a mesoporous thin film of amorphous TiO_2 impregnated with silver salt. The mesoporous titania film is elaborated by a sol-gel process. The sol contains titanium tetraisopropoxide (TTIP, Aldrich; 97%), acetylacetone (AcAc, Aldrich; 99%), hydrochloric acid (HCl, Roth; 37%), ethanol (EtOH, Carlo Erba; absolute), P123 ($(PEO)_{20}(PPO)_{70}(PEO)_{20}$, Aldrich; MW: 5000) and de-ionized water (H_2O) with the following molar ratios: TTIP/P123/ethanol/HCl/H_2O/AcAc = 1:0.025:28.5:0.015:29.97:0.5. Films are dip-coated and calcined at 340°C to form mesoporous titania films.

Silver ions are introduced within the mesopority by soaking the films in an aqueous ammoniacal silver nitrate solution. The films are then rinsed with ultrapure water and dried at room temperature for at least 12 hours.

3.2. FIB/SEM tomography.

A movie in supplementary information shows a 3D reconstruction of a sample (λ_L=514 nm, P_i=240 mW, v=3 mm.s^{-1}) analyzed with a dual-beam focused ion beam (FIB)/SEM system (Carl Zeiss Nvision40). Tomography was performed by removing 1015 successive slabs (3.8 nm in thickness in the y-direction) of matter with a Ga^+ ionic gun, and acquiring micrographs of the fresh cross-sections sequentially revealed.[33] The reconstructed volume shown in the video is about 5.6 x 3.86 x 0.52 µm^3 – x y z, with a resolution of 3 x 3,8 x 3 nm^3. A segmentation has been performed for a better identification of the different phases: the TiO_2 film about 120 nm-thick after exposure is in green, the silver-nanoparticle grating in pink and the glass substrate in blue. The apparent

roughness of the TiO_2 top surface is due to the interaction of the FIB ion beam with the thin gold layer deposited prior to the analysis to prevent charge effects in the microscope.

3.3. Electromagnetic modeling of the waveguiding metallic photonic crystal.

The grating electromagnetic modeling of Fig. 3b-d was carried out using the differential method,[29] with Li's improvement[30] for the ⊥ case. The nanoparticle lines were replaced by homogeneous 35 x 35 nm² lines with an effective refractive index calculated as for a composite material made of 50 % TiO_2 and 50 % bulk silver[34] from the average dielectric function ε for the // polarization and the average of 1/ε for the ⊥ polarization. To obtain a good agreement with experimental data, in particular for the position and contrast of both plasmon and waveguide resonances, the dispersion of TiO_2 was taken into account according to the Shimizu's data.[35] Outside the composite lines, the matrix was assumed to be composed of TiO_2 loaded with small silver nanoparticles of radius 4 nm at a 3.10^4 NP/µm^3 density. Its refractive index was deduced from the Maxwell-Garnett theory using for the refractive index of small Ag nanoparticles the expression of the dielectric function of bulk silver, corrected in size taking into account the classical free path effect.[39] The overall TiO_2 thickness was 155 nm. A constant absorption coefficient was also applied to TiO_2 to take into account losses caused by scattering by the nanocrystals. Note that no fitted parameters have been included except that small additional loss Δk = 0.02. It broadens and reduces the amplitude of the waveguide resonance to better fit the experimental data. This modeling does not really consider the wide nanoparticle size distribution and cannot accurately describe the shape of the plasmon band.

distributed collection of small nanoparticles. Indeed, $\left\langle \tilde{\chi}_{NP} \right\rangle$ is the amplitude of the periodic modulation of the NP distribution and, according to equation (9) it will grow exponentially with time provided that:

$$\Im m(\eta) < 0 \qquad (10)$$

Therefore, this condition (10) appears to be very crucial, and it will depend on the relative predominance of the thermal and oxidation terms, which will be discussed in more detail in another paper. We finally get the exponential growth rate $\lambda = \frac{\omega\varepsilon_0}{2}|E_0|^2 w_{laser} I_{0v} |\Im m(\eta)|$. Therefore, according to our analysis, we expect λ to be proportional to the laser irradiance, but also to the width w_{laser} of the laser beam. This is less obvious and comes from equation (4), showing that the process is expected to be more efficient if more space is allowed to the guided wave to coherently build.

4. Conclusions

In summary, we have shown that there exist conditions so that a single homogeneous CW visible laser beam can generate the growth of periodic arrays of metal nanoparticles in a thin film containing metallic precursors initially homogeneously distributed. The film must act as a waveguide, TiO_2 is therefore useful for its high refractive index. To grow silver nanoparticles under a CW laser exposure, as it is performed in this work, high enough atomic and ionic mobilities must be reached and they are favored here by the low initial density of the mesoporous films. Both laser-induced oxidation of silver nanoparticles and thermally induced reduction of silver ions are involved in the process. The former is well known to be particularly efficient in Ag:TiO_2 systems and the latter, which is initiated by the plasmon absorption of silver nanoparticles, requires few nanoparticle seeds. The experimental and theoretical optical studies have allowed to infer that self-arrangement originates from interferences between the free-space incident radiation and guided waves. Considering the coupled-mode theory and a perturbation linked to the changes in susceptibility resulting from the nanoparticle growth under laser exposure, we proposed a model in which the perturbation and the interference contrast are shown to mutually self-enhance in a positive feedback loop and grow exponentially. The buried nanoparticle grating resulting from this complex but one-step process perpetuates during dynamic exposure without need for stabilization techniques. The formed nanostructures act as waveguiding metallic photonic crystals, in which plasmon and waveguide resonances are coupled and, whose optical properties can easily be tuned by controlling extrinsic parameters such as the wavelength, output power and focusing of the laser, or the translation speed of the sample, and intrinsic parameters such as the film thickness or the initial nanoparticle size distribution. The technique may be used to produce tunable filters with controllable color output and opens applications in polarization imaging, displays, security or lighting.

Acknowledgements

Renée Charrière is gratefully acknowledged for the optical measurements of grating periods. This work was supported by the French National Research Agency (ANR) in the framework of project PHOTOFLEX n°ANR-12-NANO-0006 and the LABEX MANUTECH-SISE (ANR-10-LABX-0075) of Université de Lyon. The authors also thank CLYM (www.clym.fr) for access to the Jeol 2010F TEM and the dual-beam FIB/SEM system (Carl Zeiss Nvision40), and the METSA network (www.metsa.fr) for financial support.

Notes

[a] Université de Lyon, F-42023 Saint-Etienne, France; CNRS, UMR 5516, Laboratoire Hubert Curien, Université Jean-Monnet, 18 rue Pr. Lauras F-42000 Saint-Etienne. E-mail: nathalie.destouches@univ-st-etienne.fr
[b] IMEP-LAHC, Minatec, Grenoble-INP, CNRS- UMR 5130, F-38016 Grenoble.
[c] MATEIS, UMR 5510 CNRS, Université de Lyon, INSA-Lyon, 7 avenue Jean Capelle, F-69621 Villeurbanne.
Electronic Supplementary Information (ESI) available: Movie showing the 3D reconstruction of the sample top layers obtained from FIB/SEM characterizations. See DOI: 10.1039/b000000x/

References

1 S. Benedetti, F. Stavale, S. Valeri, C. Noguera, H.-J. Freund, J. Goniakowski and N. Nilius, *Adv. Funct. Mater.,* 2013, **23**, 75-80.
2 (a) T. K. Sau and A. L. Rogach, *Adv. Mater.*, 2010, **22**, 1781-1804. (b) T. K. Sau, A. L. Rogach, F. Jackel, T. A. Klar and J. Feldmann, Adv. Mater. 2010, **22**, 1805-1825.
3 S. K. Ghosh and T. Pal, *Chem. Rev.*, 2007, **107**, 4797-4862.

4 N. J. Halas, S. Lal, W.-S. Chang, S. Link and P. Nordlander, *Chem. Rev.*, 2011, **111**, 3913–3961.
5 M. Février, P. Gogol, A. Aassime, R. Mégy, C. Delacour, A. Chelnokov, A. Apuzzo, S. Blaize, J.-M. Lourtioz and B. Dagens, *Nano Lett.*, 2012, **12**, 1032–1037.
6 J. Sancho-Parramon, *Opt. Lett.*, 2011, **36**, 3527-3529.
7 W. Rechberger, A. Hohenau, A. Leitner, J. R. Krenn, B. Lamprecht and F. R. Aussenegg, *Opt. Commun.*, 2003, **220**, 137-141.
8 B. Lamprecht, G. Schider, R. T. Lechner, H. Ditlbacher, J. R. Krenn, A. Leitner and F. R. Aussenegg, *Phys. Rev. Lett.*, 2000, **84**, 4721-4724.
9 A. Christ, S. G. Tikhodeev, N. A. Gippius, J. Kuhl and H. Giessen, *Phys. Rev. Lett.*, 2003, **91**, 183901-1:4.
10 Y. Shimotsuma, M. Sakakura, P. G. Kazansky, M. Beresna, J. Qiu, K. Miura and K. Hirao, *Adv. Mater.*, 2010, **22**, 4039–4043.
11 J. Yaoa, C. Zhanga, H. Liua, Q. Daia, L. Wua, S. Lana, A. Venu Gopalb, V. A. Trofimovc and T. M. Lysakc, *Appl. Surf. Sci.*, 2012, **258**, 7625– 7632.
12 Y. Shimotsuma, M. Sakakura, P. G. Kazansky, M. Beresna, J. Qiu, K. Miura and K. Hirao, *Adv. Mater.*, 2010, **22**, 4039–4043.
13 B. Dusser, Z. Sagan, H. Soder, N. Faure, J. P. Colombier, M. Jourlin and E. Audouard, *Opt. Express*, 2010, **18**, 2913–2924.
14 M. Birnbaum, *J. Appl. Phys.*, 1965, **36**, 3688–3689.
15 J. E. Sipe, J. F. Young, J. S. Preston and H. M. Van Driel, *Phys. Rev. B*, 1983, **27**, 1141-1154.
16 F. Garrelie, J. P. Colombier, F. Pigeon, S. Tonchev, N. Faure, M. Bounhalli, S. Reynaud and O. Parriaux, *Opt. Express*, 2011, **19**, 9035–9043.
17 A. M. Prokhorov, V. A. Sychugov, V. A. Tishchenko and A. A. Khakimov, *Sov. Tech. Phys. Lett.*, 1982, **8**, 415-416.
18 M. Kaempfe, H. Graener, A. Kiesow and A. Heilmann, *Appl. Phys. Lett.*, 2001, **79**, 1876 –1878.
19 K. Loeschner, G. Seifert and A. Heilmann, *J. Appl. Phys.*, 2010, **108**, 073114–073114–10.
20 L. Nadar, R. Sayah, F. Vocanson, N. Crespo-Monteiro, A. Boukenter, S. Sao Joao and N. Destouches, *Photochem. Photobiol. Sci.*, 2011, **10**, 1810–1816.
21 N. Crespo-Monteiro, N. Destouches, L. Saviot, S. Reynaud, T. Epicier, E. Gamet, L. Bois and A. Boukenter, *J. Phys. Chem. C*, 2012, **116**, 26857–26864.
22 Y. Ohko, T. Tatsuma, T. Fujii, K. Naoi, C. Niwa, Y. Kubota and A. Fujishima, *Nat. Mat.*, 2003, **2**, 29–31.
23 N. Crespo-Monteiro, N. Destouches, L. Bois, F. Chassagneux, S. Reynaud and T. Fournel, *Adv. Mater.*, 2010, **22**, 3166–3170.
24 L. Nadar, N. Destouches, N. Crespo-Monteiro, R. Sayah, F. Vocanson, S. Reynaud and Y. Lefkir, *J. Nanopart. Res.*, 2013, **15**, 2048-2057.
25 N. J. Halas, S. Lal, W.-S. Chang, S. Link and P. Nordlander, *Chem. Rev.*, 2011, **111**, 3913–3961.
26 S. G. Tikhodeev, A. L. Yablonskii, E. A. Muljarov, N. A. Gippius and T Ishihara, *Phys. Rev. B*, 2002, **66**, 045102-1:17.
27 N. Destouches, J. C. Pommier, O. Parriaux, T. Clausnitzer, N. Lyndin and S. Tonchev, *Opt. Express*, 2006, **14**, 12613–12622.
28 D. Nau, A. Schönhardt, Ch. Bauer, A. Christ, T. Zentgraf, J. Kuhl, M. W. Klein and H. Giessen, *Phys. Rev. Lett.*, 2007, **98**, 133902:1-4.
29 R. Petit and L. C. Botten, Electromagnetic theory of gratings. (Springer-Verlag, 1980).
30 L. Li, *J. Opt. Soc. Am. A*, 1996, **13**, 1870–1876.
31 B. Luk'yanchuk, N. Zheludev, S. Maier, N. J. Halas, P. Nordlander, H. Giessen and C.T. Chong, *Nat. Mater.*, 2010, **9**, 707-715.
32 A. Yariv, *IEEE J. Quant. Electron.*, 1973, **9**, 9, 919-933.
33 L. Holzer, F. Indutnyi, P. H. Gasser, B. Münch and M. Wegmann, *J. Microsc.*, 2004, **216**, 84-95.
34 E. D. Palik, Handbook of Optical Constants of Solids. 1, (Academic Press, 1985).
35 W. Shimizu, S. Nakamura, T. Sato and Y. Murakami, *Langmuir*, 2012, **28**, 12245–12255.
36 Y. Battie, N. Destouches, L. Bois, F. Chassagneux, A. Tishchenko, S. Parola and A. Boukenter, *J. Phys. Chem. C*, 2010, **114**, 8679–8687.